

Rotation periods for very low mass stars in Praesepe

Alexander Scholz^{1*}, Jonathan Irwin², Jerome Bouvier³, Brigitta M. Sipőcz⁴,
Simon Hodgkin⁵, Jochen Eislöffel⁶

¹ *School of Cosmic Physics, Dublin Institute for Advanced Studies, 31 Fitzwilliam Place, Dublin 2, Ireland*

² *Harvard-Smithsonian Center for Astrophysics, 60 Garden St., Cambridge, MA 02138, USA*

³ *Laboratoire d'Astrophysique, Observatoire de Grenoble, BP 53, F-38041 Grenoble Cedex 9, France*

⁴ *Centre for Astrophysics Research, University of Hertfordshire, Hatfield, AL10 9AB, UK*

⁵ *Institute of Astronomy, University of Cambridge, Madingley Road, Cambridge CB3 0HA, UK*

⁶ *Thüringer Landessternwarte Tautenburg, Sternwarte 5, D-07778 Tautenburg, Germany*

Accepted. Received.

ABSTRACT

We investigate the rotation periods of fully convective very low mass stars (VLM, $M < 0.3 M_{\odot}$), with the aim to derive empirical constraints for the spindown due to magnetically driven stellar winds. Our analysis is based on a new sample of rotation periods in the main-sequence cluster Praesepe (age 600 Myr). From photometric lightcurves obtained with the Isaac Newton Telescope, we measure rotation periods for 49 objects, among them 26 in the VLM domain. This enlarges the period sample in this mass and age regime by a factor of 6. Almost all VLM objects in our sample are fast rotators with periods < 2.5 d, in contrast to the stars with $M > 0.6 M_{\odot}$ in this cluster which have periods of 7–14 d. Thus, we confirm that the period-mass distribution in Praesepe exhibits a radical break at $M \sim 0.3 - 0.6 M_{\odot}$. Our data indicate a positive period-mass trend in the VLM regime, similar to younger clusters. In addition, the scatter of the periods increases with mass. For the $M > 0.3 M_{\odot}$ objects in our sample the period distribution is probably affected by binarity. By comparing the Praesepe periods with literature samples in the cluster NGC2516 (age ~ 150 Myr) we constrain the spindown in the VLM regime. An exponential rotational braking law $P \propto \exp(t/\tau)$ with a mass-dependent τ is required to reproduce the data. The spindown timescale τ increases steeply towards lower masses; we derive $\tau \sim 0.5$ Gyr for $0.3 M_{\odot}$ and > 1 Gyr for $0.1 M_{\odot}$. These constraints are consistent with the current paradigm of the spindown due to wind braking. We discuss possible physical origins of this behaviour and prospects for future work.

Key words: stars: low-mass, brown dwarfs, stars: rotation, stars: evolution, stars: activity

1 INTRODUCTION

The spin of stars is a strong function of stellar mass and age. The age-dependence for main-sequence F-K-type stars has been empirically established in the seminal paper by Skumanich (1972) as $\omega \propto t^{1/2}$. Originally found from rotational velocities in the Pleiades and Hyades, this relation still holds asymptotically on the main-sequence when evaluated with the large sets of rotation periods in open clusters that is currently available. Most recent tests of the Skumanich law tend to give slightly higher power law exponents of 0.56 (Collier Cameron et al. 2009) or 0.52 (Barnes 2007).

From the theory side, the Skumanich law has been reproduced in the prescription provided by Kawaler (1988),

which is based on the analytical wind model by Mestel (1984). Under plausible assumptions (linear dynamo, magnetic field a mixture between dipolar and radial), the Kawaler expression simplifies to $dJ/dt \propto \omega^3$, which gives the desired $\omega \propto t^{-1/2}$ behaviour. Recent numerical work, however, indicates that the Kawaler-type wind parameterisation may not be an adequate explanation for the empirically found Skumanich law (Matt & Pudritz 2008).

F-K-type stars exhibit a well-studied rotation-mass relation on the main-sequence. For example, at the age of the Hyades the rotation periods increase steadily towards later spectral types, from 5 d for late F-stars to 12 d for late K-stars (Radick et al. 1987). This relation is remarkably tight and it seems possible to explain the few outliers as tidally locked binaries or as objects with specific spot configurations resulting in a wrong period measurement. Thus, for

* E-mail: aleks@cp.dias.ie

these objects mass and age essentially fix the rotation rate, which allows for the possibility of 'gyrochronology', i.e. measuring ages from rotation periods (Barnes 2007).

Observations have not been able yet to establish similarly robust age/mass-rotation dependencies for the very low mass stars in the M-type regime. It is clear that the F-K-type period-mass relation breaks down in the early-M regime, corresponding to a mass threshold of $0.3\text{-}0.5 M_{\odot}$. This is most readily seen from the M-dwarfs periods in Praesepe (Scholz & Eislöffel 2007), which are 1-3 d, much shorter than in the K-type regime, and from the rotational velocity data, which indicates a significant increase in the rotation rate between early to mid M-types (e.g., Delfosse et al. 1998; Jenkins et al. 2009).

Similarly, the Skumanich-type rotational braking does not hold anymore for VLM objects with $M < 0.3 M_{\odot}$. While angular momentum losses occur in this mass regime as well, the stars tend to maintain high rotation rates over Gyrs, which is not consistent with the $\omega \propto t^{-1/2}$ spindown. Most commonly the VLM spindown is empirically described with an exponential braking law $\omega \propto \exp(-t/\tau)$.

This exponential behaviour is primarily motivated by the theoretical framework by Kawaler (1988), see above. In a modification suggested by Chaboyer et al. (1995), stars above a critical threshold $\omega > \omega_{\text{crit}}$ are treated with $dJ/dt \propto \omega_{\text{crit}}^2 \omega$, which results in an exponential spindown law. To be able to match the period data in open clusters, ω_{crit} has to be assumed to be a function of mass (e.g. Krishnamurthi et al. 1997; Irwin et al. 2007). Empirically, however, the form of the spindown law is poorly constrained. For recent reviews on these subjects, see Scholz (2009) and Irwin & Bouvier (2009).

In this paper we set out to investigate the period-mass and period-age relation for fully convective very low mass stars based on a new set of rotation periods measured for members of the open cluster Praesepe. Praesepe, at an age of ~ 600 Myr, is an important cluster to constrain the spindown law, because the effect of wind braking can be studied in isolation. So far, however, only a very small sample of 4 periods was available for evolved VLM stars in open clusters (Scholz & Eislöffel 2007). Our goal here is to provide a quantitative measurement of the VLM spindown law based on a significantly larger sample of periods.

2 PHOTOMETRIC MONITORING

2.1 Observations

Photometric monitoring observations of Praesepe were made with the 2.4 m Isaac Newton Telescope (INT, La Palma), during the nights of 19th-27th January 2010. Data were obtained on 8 out of the 9 nights. The INT was equipped with the Wide Field Camera (WFC), mounted at prime focus. The INT WFC provides a field of view of approximately $34' \times 34'$ over a mosaic of four $2k \times 4k$ pixel CCDs, with $\sim 0''.33$ pixels. We selected 4 contiguous fields (with minimal overlap) around the centre of the cluster, such that the central pixels of chip 4 fell on the positions given in Table 1.

All observations were made with the SDSS-*i* filter which suffers rather less from fringing than the other, broader, I-

Table 1. Field central coordinates and number of long/short exposures per field

Field	RA (J2000)	DEC (J2000)	Nlong*	Nshort*
1	8:42:10.4	19:27:54	96	99
2	8:39:44.8	19:27:54	97	95
3	8:42:10.4	20:02:06	96	94
4	8:39:44.8	20:02:06	93	94

* number of epochs in the final lightcurves after rejecting a few images obviously affected by bad guiding or clouds

Table 2. Dates of observations with number of exposures for each integration time and comments

Date	N300	N20	N100	Comments
2010-01-19	53	56	0	clear
2010-01-20	57	63	0	clear
2010-01-21	57	57	0	cirrus
2010-01-22	47	46	0	cirrus, humid
2010-01-23	60	64	0	clear
2010-01-24	60	68	0	clear
2010-01-25	12	12	0	clear
2010-01-26	0	0	0	clear, humid, bad seeing
2010-01-27	0	20	49	cirrus, variable seeing

band filters available for the INT WFC. For every exposure, we tried to ensure that the same guide-star was centred on the same guide-pixel. This adds a small overhead to our observing cadence, but has the advantage of minimizing photometric systematics arising from drifts in the telescope pointing between and during exposures. Exposures were alternated between short and long integration times of 20 s and 300 s, allowing us to measure the more massive members of the cluster which would saturate in the long exposures. Our average observing cadence per-star is 29.9 min (i.e. the time to complete a cycle of short and long exposures round all four fields). On one night the full moon was very close to Praesepe, and 3×100 s exposures were used in place of a single long exposure. Conditions on the whole were good for La Palma in winter, with a median seeing of $1''.36$ arcseconds for our Praesepe observations, and a median ellipticity of 0.09 measured from the stellar images. Most nights were reasonably clear, with intermittent thin cirrus appearing throughout the run, and occasional periods of high humidity forcing us to close the dome. Photometric standards were measured at the start and end (and occasionally in the middle) of each night to enable us to transform our *i*-band photometry into the Johnson-Cousins system. Our observations are summarised on a night-by-night basis in Table 2.

2.2 From images to lightcurves

The data reduction steps are described in full elsewhere (Irwin et al. 2007). In summary, for the 2-D processing (bias correction, flatfielding, defringing), and astrometric and photometric calibration of each WFC exposure, we used a pipeline developed by the Cambridge Astronomical Survey Unit (CASU). Next, two *master images* (one for the short exposures and one for the long exposures) were made for each of the four Praesepe pointings by stacking 10 of

our best images. From these we generated *master catalogues* which contain all the sources and their coordinates for which we measure list-driven aperture photometry from each of the short and long exposures. Each source has an associated morphological classification, and a flag indicating the degree to which it is blended (based on an analysis of overlapping isophotes).

Lightcurves were constructed for ~ 47000 objects, of which ~ 13500 have stellar shape parameters. To calibrate each epoch, we fit a 2-D quadratic polynomial to the residuals in each frame (measured for each object as the difference between its magnitude on the frame in question and the median calculated across all frames) as a function of position, for each of the 4 WFC CCDs separately. Subsequent removal of this function accounted for effects such as varying differential atmospheric extinction across each frame. Over a single WFC CCD, the spatially-varying part of the correction remains small, typically 0.02 mag peak-to-peak (Irwin et al. 2007).

We show the *RMS* diagrams for the stellar sources in the long and short exposures in Fig. 1. For the long exposures we achieve a photometric precision of 1-2 mmag for the brightest objects at $i = 15.5$ (stars brighter than this are saturated), with *RMS* scatter $< 1\%$ for $i \leq 19$. For the short exposures we achieve *RMS*=1-2 mmag at $i = 13.0$ and about 4 mmag at $i = 15.5$.

We cross-checked our lightcurve database with the member lists published in Hambly et al. (1995) and Kraus & Hillenbrand (2007, KH in the following). 381 of our lightcurves belong to one of their member candidates. This total sample contains 170 duplications, which are detected in the long and the short exposures, i.e. the number of cluster members covered by our survey is 211.

3 PERIOD SEARCH

The main goal of this study is to derive rotation periods from photometric monitoring. Therefore we searched for the presence of periodicities in the lightcurves of the 211 objects which are known members based on colours and proper motion. The duplicates which are measured in short and long exposures provide a useful cross-check for the periods.

We use four independently developed period search routines. Three of the algorithms are based on Fourier-like periodograms, but they differ in the implementation of the periodograms and the way the best periods are selected. The fourth one is based on the string length method. In addition, each of the four period searches includes a visual check of the phased lightcurves. In our study, this procedure is done by three researchers separately, which should minimize the subjectiveness of the results. In the following we will briefly explain the different routines.

3.1 Monitor

Here we follow the method described in Irwin et al. (2006). We adopt as the null hypothesis a model of a constant magnitude, and compare this to the alternate hypothesis that the light curve contains a sinusoidal modulation, of the form:

$$m_1(t) = m_{dc} + \alpha \sin(\omega t + \phi) \quad (1)$$

where α and ϕ represent the semi-amplitude and phase of the sinusoid, and $\omega = 2\pi/P$ is the angular frequency corresponding to rotation period P . In order to determine the period, we fit this model using standard linear least-squares, at discrete values of ω sampled on a uniform grid in frequency from 0.01 to 100 d. To judge the significance of each period, we calculate the χ^2 improvement of the sinusoidal model relative to the null hypothesis ($\Delta\chi^2$).

Due to the small sample size, we omit the cut in $\Delta\chi^2$ used by Irwin et al. (2006), and simply subjected all of the light curves to eyeball examination, to define the final sample of periodic variables. 65 light curves fulfill these criteria. Several objects are identified which appeared to be varying, but the period was poorly-determined due to less than a cycle being seen; these are excluded, as are the remaining cluster members, the majority of which consistent with no variation. The sample of 65 periods contains 18 duplicates; this leaves 47 good periods, all shorter than 6 d. For the duplicates we adopt the period with maximum $\Delta\chi^2$.

3.2 SE2004

This set of routines is based on the period search as first published in Scholz & Eislöffel (2004a, SE2004) and further discussed in Scholz & Eislöffel (2004b, 2005). In a first step, the routine eliminates 3σ outliers from the lightcurves. Next, we identify the highest peak in the Scargle periodogram for unevenly sampled lightcurves (Scargle 1982). For this peak we calculate a false alarm probability following the relation by Horne & Baliunas (1986). For the best period from the Scargle periodogram, a phaseplot is calculated (lightcurve as a function of phase). We subtract the period modeled as a sinecurve and compare the variance in the original lightcurve with the variance in the residuals using the F-test. Finally the CLEANed periodogram is computed using the routines by Roberts et al. (1987). We accept a period if the Scargle FAP is $< 1\%$, the F-test FAP is $< 5\%$, and the highest peak in the Scargle periodogram is among the highest in the CLEAN periodogram. In addition, the phaseplots for all 381 lightcurves are visually inspected.

Using the method as outlined in SE2004, we estimate the range of periods we are able to detect. For 10 non-variable objects with Gaussian noise, we artificially add periods ranging from 0.05 to 10 d and try to recover them using the same combination of Scargle periodogram and F-test as outlined above. From this test it is obvious that the analysis is sensitive to periods $P < 6$ d and becomes unreliable (deviation between imposed and measured period $> 10\%$) for longer periods.

In the catalogue of 381 objects, 222 fulfill the FAP criteria given above. We exclude the 99 periods longer than our upper limit of 6 d and 15 periods for bright sources affected by saturation ($J < 10$ mag). From the remaining 108, 82 pass the visual inspection. 25 of the objects with periods are duplicates; two of them have inconsistent periods and are excluded. For the duplicates with consistent period, we adopt the one measured with higher Scargle power. In total, this method yields 55 good periods.

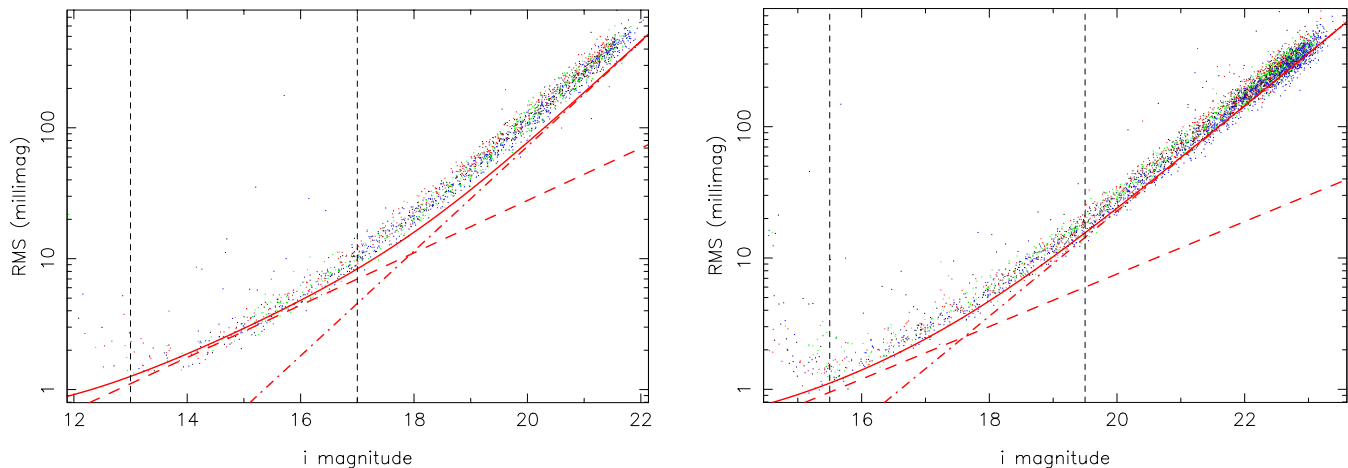


Figure 1. *RMS* versus magnitude for *i*-band photometric monitoring in one of the Praesepe fields for the short (20s, left) and long (300s, right) exposures. Only unblended objects with stellar morphology are shown as dots, colour-coded by detector. The solid line shows the overall predicted *RMS*, combining contributions from sky noise (dot-dashed line) and object photon counting noise (dashed line). The error in the sky background fitting is not included here which explains why the predicted *RMS* underestimates the measurements at the faint end. The vertical lines indicate the magnitude range from which we identify non-variable stars for performing the frame-to-frame photometric calibration.

3.3 CLEAN and String-Length

Here we discuss the period search using the CLEAN discrete Fourier transform (CLN, Roberts et al. 1987) and string-length (SL, Dworetzky 1983) methods. Periods are searched over the range from $P_{\min} = 0.1$ to $P_{\max} = 6$ d by sampling the frequency range uniformly with increments of $5 \cdot 10^{-3}$ cycles/day. Light curves folded in phase with the best periods derived from the 2 methods are visually inspected to estimate the reliability of the reported period. We rank the results in 3 groups: clearly periodic light curves, possibly periodic ones, and non-periodic ones.

The CLN analysis of 381 light curves yields robust periods for 47 light curves, while possible periods are found for 23 additional light curves. The remaining 311 light curves do not show evidence for periodic variations. After duplicate removal, we are left with 54 periods from CLN, from which 12 are measured twice consistently. The majority of these periods (38/54) are classified as robust after eyeballing.

The SL method applied to our sample yields robust periods for 18 light curves, of which 15 are also found and classified as robust from the CLN method. The SL method additionally yields 13 possible periods, of which 5 are detected as robust periods in the CLN analysis, sometimes as aliases. After duplicate removal 24 periods remain from the SL method, from which 7 are measured twice consistently.

3.4 Combining the four period samples

The application of four different period search routines and the presence of a significant sample of duplicates measured in short and long exposures gives us a good handle on the robustness of our results. In general, when two lightcurves are available for the same object, the agreement is usually excellent within the same period search routine. Typical deviations are $< 2\%$ with few outliers. Thus, all four period routines are internally consistent and provide accuracies in the range of 1%.

In Table 3 we list our final sample of 49 periods. For a period to appear in this table, it had to be registered at least in two different period search routines. In the final column of the table we summarise the results of the period search using a four digit flag. Each digit gives the number of consistent period measurements for this object for each of the four algorithms in the order as described above, i.e. Monitor, SE2004, CLN, SL. Adding these four digits indicates how often a given period has been measured consistently. The phased lightcurves for these 49 periods are shown in Fig. 5 and 6 in the same order as in the table.

In addition, the period search yields 24 periods which are only detected once (sum of the flags in Table 3 would be 1). These mostly have dodgy phaseplots and are considered to be unreliable. Moreover, these periods do not follow the trends reported in the mass-period diagram (Sect. 4) and include a substantial sample of long periods > 6 d which we do not consider to be trustworthy.

The comparison of the four independent period samples shows some noteworthy trends. First, there is a group of objects for which the same period is reliably recovered by several algorithms ($\text{flag} \geq 4$). While re-assuring, this sample amounts only to one half of the total number of periods we consider to be trustworthy. This is mostly due to the fact that the string length method is not as sensitive as the periodogram techniques and misses a substantial number of periods which are measured with high confidence by multiple periodogram-based algorithms. In addition, we have 5 ‘string length outliers’, i.e. objects for which consistent periods are measured by multiple periodogram techniques but the string length methods provides a different result (objects KH791, 569, 603, 957, 894). For all five cases, the SL period is close to a harmonic of the periodogram period; the ratios between periodogram period and SL period are approximately 5/2, 3, 1/2, 3, 4/3. In these cases, we adopt the result from the periodogram technique.

When the same object has a period from different periodogram techniques, the agreement is excellent. We have

only three cases with deviating results, two of them appear in the final sample in Table 3 because one period has been measured more than once (KH737, KH912). Excluding these outliers, the average deviations are 0.5%. For comparison, the average deviation between periods from periodograms and periods from the string length method is, for objects with consistent periods, 1.2%. In Table 3 we adopt the periods determined from periodograms, i.e. the string length result is used as a consistency check. The substantial samples of objects with only one detection are mainly due to the subjective nature of the eyeballing.

In Table 3 we additionally give an estimate of the peak-to-peak amplitude for the periodic lightcurves. This has been determined by a) fitting the lightcurve with a sine function and b) calculating the peak-to-peak amplitude of this function. By using the sine function instead of the actual lightcurve, we correct for the effect of the noise on the amplitude. These amplitudes range from 0.01 to 0.04 mag, with a few outliers with higher values. They do not show any correlation with brightness or period.

4 ROTATION VS. MASS

For all objects with periods we estimated masses by comparing the J-band magnitudes from 2MASS, converted to the CIT system, with the BCAF98 model isochrone for 630 Myr from Baraffe et al. (1998). As the magnitudes are constant within 5% for ages between 500 and 800 Myr, these mass estimates do not depend on the particular choice of the age. The uncertainties in the models might introduce systematic errors. Therefore, our masses should only be compared with values calculated from the same model tracks. The total sample of cluster members covered by our observations contains 21, 23, 21, and 146 objects in the mass bins 0.1-0.2, 0.2-0.3, 0.3-0.4, and $> 0.4 M_{\odot}$. The 'success rate' (i.e. the fraction of objects for which we are able to measure the period) is at 48-61% for the three lowest mass bins, but only 8.9% for the higher masses. This indicates that we are missing a substantial numbers of periods for $M > 0.4 M_{\odot}$, either due to the period detection limit at ~ 6 d or due to saturation effects.

In Fig. 2 we plot the period sample as a function of object mass; the 24 most robust periods with flag ≥ 4 are marked with squares. All quantitative results in this Section are derived from these periods. The less robust periods with flag of 2-3 generally show the same distribution in this plot. In addition, we overplot the median period in the mass bins 0.1-0.2, 0.2-0.3, and 0.3-0.4 M_{\odot} with large octagons. This clearly shows a trend of faster rotation towards lower masses, in line with previous findings (Scholz & Eislöffel 2005, 2007). Below 0.3 M_{\odot} where the majority of our datapoints is found there is only one object with $P > 2.5$ d, significantly below our period detection limit (Sect. 3.2). This suggests that very low mass objects in Praesepe are generally fast rotators. The plot also reveals that the scatter in the periods in a given mass bin decreases towards lower masses. The total spread is 1.34 d for $M < 0.2 M_{\odot}$, 1.66 d for $0.2 < M < 0.3 M_{\odot}$, and 3.4 d for $0.3 < M < 0.4 M_{\odot}$.

Upon closer inspection Fig. 2 might indicate a more complex substructure. In particular, we note a dearth of datapoints for periods between 2.6 and 4.0 d, which cannot

Table 3. Periods in Praesepe: object ids from Hambly et al. (1995, HSHJ) and Kraus & Hillenbrand (2007, KH), J-band magnitude (from 2MASS, converted to CIT), mass estimate (based on J-band magnitudes), adopted period, amplitude, flag (for explanation see Sect. 3.4). With one exception at 85% (HSHJ412), all objects have membership probabilities $\geq 95\%$ according to KH. The periods are ordered by increasing mass (or decreasing J-band magnitude); flags ≥ 4 indicating the most robust periods are marked in bold.

HSHJ	KH	J-mag	M (M_{\odot})	P (d)	A (mag)	Flag
-	1117	15.95	0.12	0.683	0.024	1100
412	1036	15.31	0.16	1.754	0.040	1111
-	1013	15.20	0.16	0.693	0.041	2222
233	912	15.17	0.17	0.442	0.022	1010
-	1053	15.10	0.17	0.498	0.026	0110
-	1108	15.09	0.17	0.216	0.014	1110
396	940	15.01	0.18	0.593	0.009	1111
258	1029	14.99	0.18	0.550	0.013	1100
423	880	14.99	0.18	1.179	0.013	0211
256	975	14.99	0.18	1.754	0.010	1110
-	994	14.85	0.19	0.411	0.015	1111
-	898	14.85	0.19	1.220	0.035	2221
-	933	14.84	0.19	0.467	0.021	1212
-	842	14.71	0.21	0.580	0.015	2222
-	966	14.69	0.21	0.785	0.009	1110
370	894	14.64	0.22	1.689	0.010	1110
376	731	14.56	0.23	1.276	0.017	2210
397	793	14.54	0.23	1.232	0.025	2222
-	791	14.50	0.23	1.511	0.011	1110
-	674	14.49	0.23	2.232	0.012	1110
195	702	14.37	0.25	1.155	0.011	1210
421	886	14.33	0.25	0.284	0.006	1100
430	789	14.33	0.25	2.242	0.021	2221
428	698	14.25	0.26	1.706	0.085	2222
291	770	14.22	0.27	1.276	0.027	2221
419	647	14.20	0.27	3.996	0.010	1100
229	957	13.89	0.32	2.294	0.008	1210
368	612	13.88	0.32	4.464	0.025	2220
-	824	13.87	0.32	1.348	0.017	2212
295	658	13.82	0.33	2.646	0.072	2220
289	741	13.76	0.34	1.672	0.024	2222
436	714	13.74	0.34	4.869	0.017	2100
305	822	13.55	0.37	1.207	0.010	2201
270	557	13.55	0.37	4.291	0.015	2210
-	737	13.54	0.37	0.509	0.029	0120
267	802	13.53	0.38	1.106	0.015	1211
212	624	13.30	0.42	0.526	0.018	2020
272	637	13.25	0.42	3.982	0.012	2200
-	569	13.17	0.44	1.894	0.016	1110
285	676	13.12	0.45	5.755	0.029	1200
303	603	13.10	0.45	0.842	0.016	1200
435	524	12.99	0.47	3.968	0.035	0210
253	735	12.86	0.49	0.812	0.007	1110
425	532	12.92	0.48	1.153	0.013	0101
366	523	12.51	0.54	1.374	0.024	1110
278	361	12.16	0.60	4.274	0.050	1010
249	486	12.16	0.60	4.854	0.016	1110
-	234	11.28	0.75	5.682	0.007	0110
357	369	11.19	0.76	3.268	0.020	1110

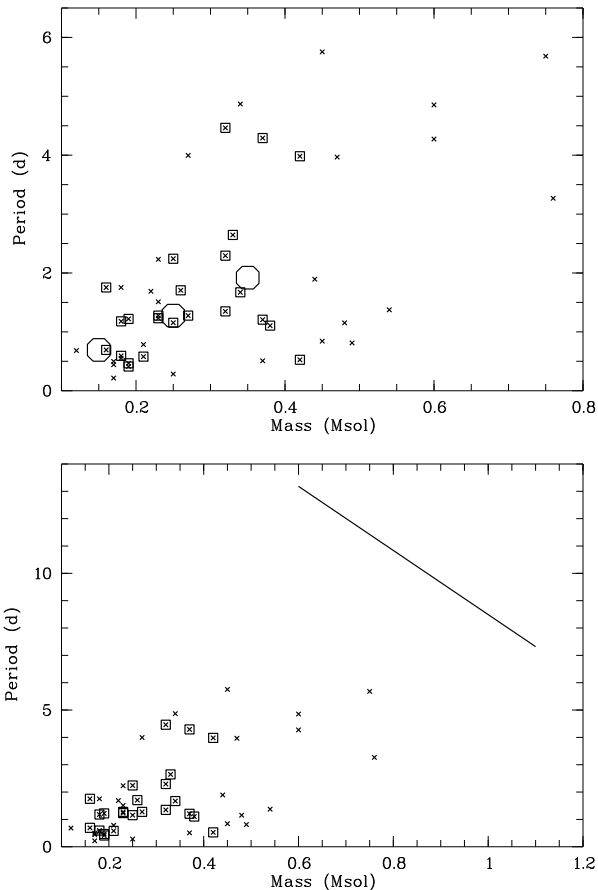


Figure 2. **Upper panel:** Rotation periods in Praesepe from our study plotted vs. mass. Periods with flag ≥ 4 (see Table 3) are marked with squares. The median periods in the mass bins 0.1-0.2, 0.2-0.3, and 0.3-0.4 M_{\odot} are plotted as octagons. **Lower panel:** Period-mass relation over the full low-mass range. The solid line shows the period-mass relation for low-mass stars in Praesepe, derived from the colour-mass relation given by Delorme et al. (2011).

be explained by a lack of sensitivity in the period search. Furthermore there may be a lack of periods around $M = 0.3 M_{\odot}$ at $P < 1$ d. A larger sample of periods is needed to verify if these features in the period-mass distribution are real or spurious.

In contrast to the VLM objects discussed here, the more massive stars in Praesepe show a tight correlation of period vs. mass which is plotted as a solid line in the lower panel of Fig. 2. To derive this relation, we converted the period-colour relation from Delorme et al. (2011) to period-mass using the 2MASS to CIT transformation from Carpenter (2001) and the linearly fitted colour-mass relation from the same BCAH98 isochrone used for our sample. The standard deviation around this relation is 0.46 d, according to Delorme et al. (2011), i.e. the scatter at a given mass is much smaller than for VLM objects.

The transition from the period-mass relation for 0.6-1.2 M_{\odot} stars and the VLM regime is not fully covered yet by the existing surveys. This regime is difficult to observe because it requires deep monitoring over timescales of 2-15 d. It is clear, however, that between 0.35 and 0.6 M_{\odot}

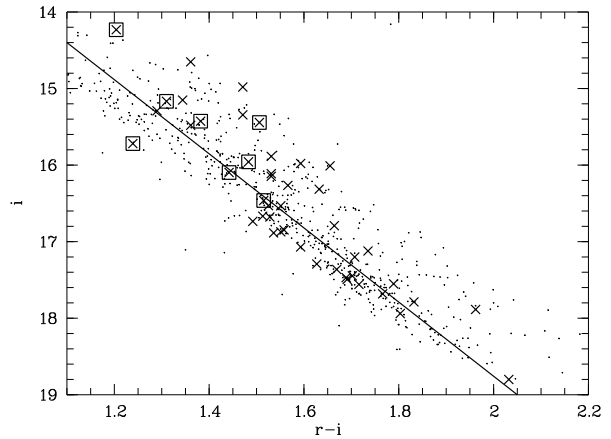


Figure 3. Colour-magnitude diagram for Praesepe members from the KH survey, based on photometry from the Sloan Digital Sky Survey (Abazajian et al. 2009). Objects with measured period from Table 3 are shown with crosses; slow rotators ($P > 3$ d) are marked with squares. Two objects with periods (KH369 and KH361), both slow rotators, are at $i < 14$ and $r - i < 1.0$ and are not shown here. For two more (KH1013 and KH234) no valid i-band photometry is available. The solid line marks the assumed limit of the single star sequence.

the periods increase strongly with mass, as already stated by Scholz & Eislöffel (2007). Some of our objects at $M > 0.3 M_{\odot}$ with relatively long periods might be objects in transition between the two domains.

Two other properties might have an additional effect on the distribution of datapoints in Fig. 2, the configuration of the spots and binarity. Some objects could have specific spot configurations resulting in an erroneous period measurement. The simplest case for such a configuration is two equally sized spots with a longitude difference of 180 deg. In this scenario these objects would have true rotation periods twice the measured periods. This could explain some of the scatter in Fig. 2.

The effects of binarity are twofold. On one side, we would overestimate their masses. For example, an equal-mass binary with 0.35 M_{\odot} components would be falsely estimated to have a mass of $\sim 0.47 M_{\odot}$. On the other hand, close binaries might be tidally locked and thus faster rotating than coeval single stars.

As binaries are expected to be brighter than single stars of the same colour, a colour-magnitude diagram as shown in Fig. 3 can be used to test for the presence of binaries in our period sample. The distribution of Praesepe members from KH in colour-magnitude space shows an obvious cumulation at the blue side, interpreted as the single star sequence. We approximate this sequence with a straight line and shift it slightly to the red to estimate the fraction of binaries. Based on this boundary line, the total sample of Praesepe members in Fig. 3 has a binary fraction of 351/673 (52%), almost identical to the value derived by Hodgkin et al. (1999) using a similar approach. This ratio is slightly magnitude dependent; for $i < 16.5$ we find a higher binary fraction of 61% compared with 45% for the fainter objects.

From Fig. 3 it seems clear that the objects with periods which are brighter than $i \sim 16.5$ exhibit a significantly higher binary fraction than the fainter ones. We find a bi-

nary fraction of $8/24$ ($33 \pm 12\%$) for $i > 16.5$, which is lower, but still consistent with the value for the total sample of members. For the objects with $i < 16.5$ the fraction is $18/21$ ($86 \pm 7_2\%$), significantly higher than in the total sample. While the reported binary fractions depend somewhat on the choice of the boundary between single and binary sequence and should be taken with caution, the *increased* binary fraction for the periodic objects at $i < 16.5$ is robust against variations in this boundary.

This finding might help to explain why the scatter in the periods increases with mass (Fig. 2). The *i*-band limit of 16.5 mag corresponds to a mass of $\sim 0.3 M_\odot$. Above this limit, where we expect most objects to be binaries, the scatter is roughly twice as large as below. Some of them could be spun up tidally locked binaries and thus appear at shorter periods than single stars. It is conceivable that most of the single stars at these masses are rotating with periods longer than our detection limit, in line with the period-mass correlation seen at $0.6\text{--}1.2 M_\odot$ (solid line in Fig. 2).

Apart from binarity, an alternative explanation for the distribution of the periodic objects in Fig. 3 is the ‘blue dwarf phenomenon’ described by Stauffer et al. (2003) for the Pleiades and by Hartman et al. (2009) for M37, a cluster similar in age to Praesepe. The paper by Hartman et al. (2009) shows that ‘at fixed luminosity rapidly rotating late K and early M dwarfs tend to be (...) redder in $(V - I_C)$ than slowly rotating dwarfs’. This is attributed to increased stellar activity in the fast rotators. Assuming that we are missing the slow rotators in the $i < 16.5$ range due to our period detection limit at 6 d, the effect could explain why most of the objects with periods in this magnitude range are redder than the single-object isochrone in $r - i$. A detailed assessment of these issues requires a more complete period coverage, multi-band photometry and/or spectroscopy and is beyond the scope of this paper.

5 ROTATION VS. AGE

For the analysis of the rotational evolution, we compare our period sample in Praesepe with the periods in NGC2516 (age 150 Myr), as published by Irwin et al. (2007). We select only objects with masses $< 0.3 M_\odot$. The NGC2516 sample has two outliers with periods > 4 d which are excluded. In total, we are working with 96 periods in NGC2516 and 25 in Praesepe. The lower mass limit in the two period samples is $0.1 M_\odot$. While the masses may be systematically off due to model uncertainties, they have been calculated by comparing photometry from 2MASS with the BCAH tracks in a consistent manner and are thus comparable.

We choose NGC2516 as comparison sample because it is the largest and cleanest VLM period sample at ages of 100–200 Myr. Our goal is to isolate the effect of wind braking, therefore we refrain from using younger clusters where disk braking or contraction might still play a role. The VLM period samples in M34 (Irwin et al. 2006) and Pleiades (Scholz & Eislöffel 2004b) are too small for a meaningful quantitative analysis, but are consistent with the periods in NGC2516. In M50 the period sample might be severely affected by contamination (Irwin et al. 2009).

The samples in NGC2516 and Praesepe are plotted in Fig. 4 as a function of age. Median (octagon), 10% and 90%

percentiles of the periods (horizontal lines) are overplotted. The uncertainties for the percentiles are in the range of 0.05/0.1 d for the 10/90% limit in Praesepe and 0.02 d for NGC2516. In both cases, the analysis is sensitive to periods from 0.1 to at least 5 d. Thus, both the upper and lower period limits are likely to be reliable. In Praesepe there is a clear gap around 1 d due to the strongly clumped sampling of the time series, which could indicate that the median is in fact slightly higher.

The main caveat, however, is the fact that it is more difficult to find periods at the low-mass end. Combined with the period-mass trend, this implies a possible under-representation of fast rotators in these samples. Thus, the median and the lower limit could be overestimated. This problem likely applies to both clusters in a similar way; in NGC2516 the completeness drops from 100% to 20% around $M = 0.15 M_\odot$ (Irwin et al. 2007).

We aim to reproduce the evolution of the median and the 10% and 90% percentiles by simple evolutionary tracks. We consider an exponential spindown law $P \propto \exp(t/\tau)$ (left panels in Fig. 4) and a power law $P \propto t^\alpha$ (right panels). In the upper row of Fig. 4 we attempt to fit the median and upper/lower limit with the same spindown law (i.e. with constant τ or α), whereas we allow for varying parameters in the lower row. In addition, we vary the initial period P_{ini} slightly to match the observed periods in NGC2516. Fig. 4 additionally shows the period evolution without any angular momentum loss.

For all spindown tracks, we take into account the contraction by multiplying with R/R_{ini} , where we use radii from the BCAH98 isochrones. To mimic the period-mass trend, we use the radii for an $0.3 M_\odot$ object for the period upper limit, $0.2 M_\odot$ for the median, and $0.1 M_\odot$ for the lower limit. The tracks do not significantly depend on this choice; they are mostly parallel for all three masses. As seen in the tracks without spindown, the contraction causes the rotation periods to drop by 20–30%, depending on mass.

This analysis yields two main results: First, the period evolution cannot be explained with zero rotational braking (see dotted lines in the left panel of Fig. 4). Tracks without spindown predict the median period in Praesepe to be at ~ 0.5 d, whereas the observed median is at 1.0 d. Similarly, these tracks predict an upper and lower period limit significantly lower than observed. Thus, VLM stars undergo angular momentum losses on the main-sequence.

Second, the spindown tracks with constant parameters cannot simultaneously explain the evolution of upper limit, median, and lower limit. This is seen for exponential and for power law spindown laws (dashed and dash-dotted lines in the upper panels of Fig. 4). The upper limit and the median can be reasonably well reproduced with $\tau = 500$ Myr or $\alpha = 0.6$, which is consistent with the result from Scholz & Eislöffel (2007) based on much smaller period samples. However, the lower limit requires different parameters. Simply speaking, the fast rotators in Praesepe rotate too fast to be explained by the same spindown law as the slower rotators.

There are two ways to explain this second finding. On one side it is possible that we are missing a significant population of fast rotators in NGC2516. Based on the similar time sampling and mass coverage in NGC2516 and Praesepe, this currently seems implausible. However, the small

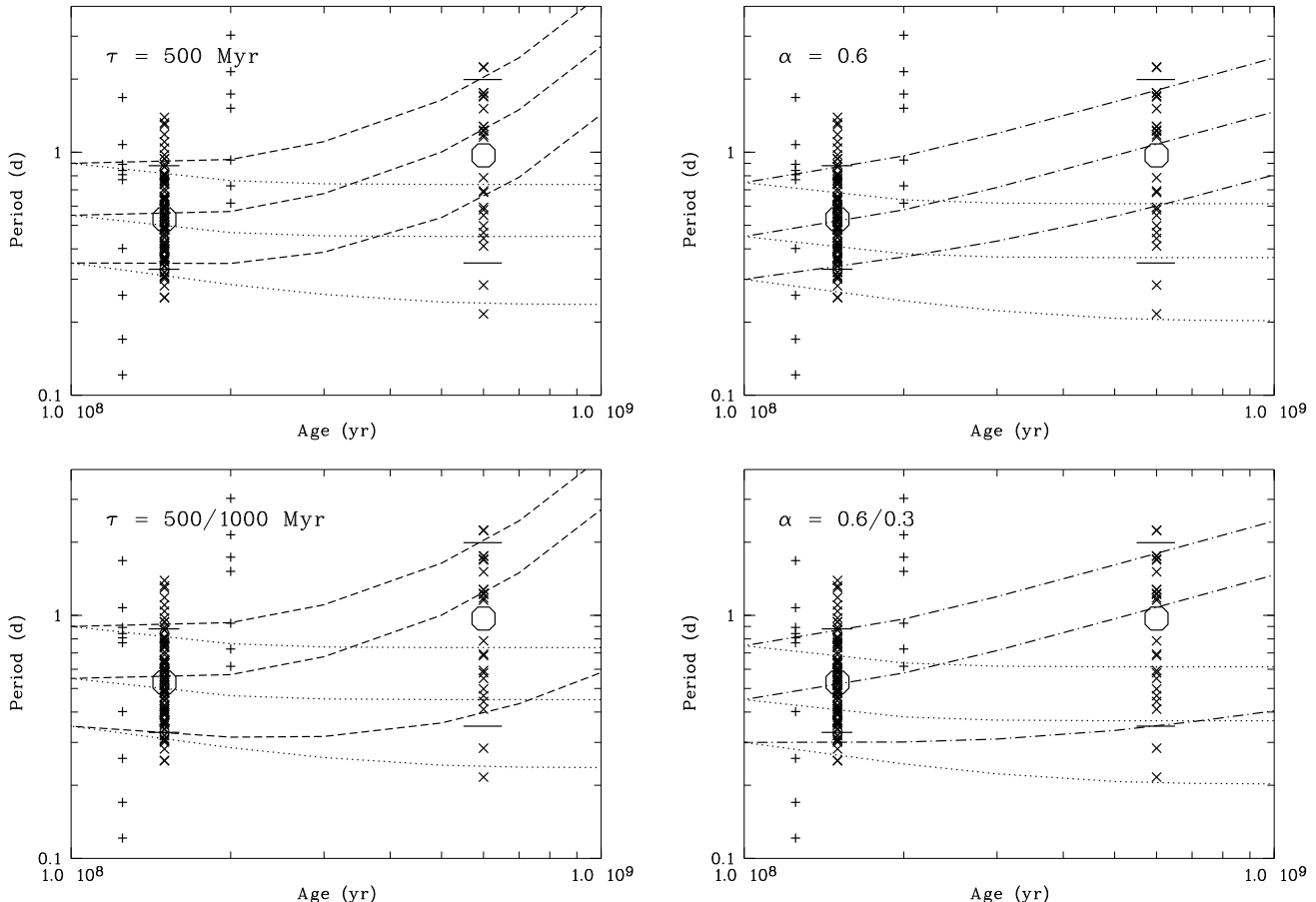


Figure 4. Rotation periods in NGC2516 and Praesepe (crosses) in comparison with spindown tracks. Dashed lines: exponential spindown; dash-dotted lines: power-law spindown; dotted lines: no spindown. Octagons show the median of the period distribution, horizontal lines the 10% and 90% percentiles of the periods. We also overplot periods in the Pleiades and M34 with plusses.

period sample in the Pleiades does contain 2 such objects with $P < 0.2$ d, out of 9 in total. A larger VLM period sample in a cluster at ~ 100 Myr would be valuable to exclude this option.

On the other side we consider the possibility that the spindown is not constant and the lower mass objects (and faster rotators) are affected by less rotational braking. In the lower panels of Fig. 4 we show exponential and power law tracks with variable τ and α . For the median and the upper limit we take the same parameters as before, but for the lower period limit we use $\tau = 1000$ Myr and $\alpha = 0.3$. The plot shows that this choice of parameters matches the data quite well. Thus, it is plausible that the spindown law in the VLM regime is a function of stellar mass.

It should be noted that the choice of $\tau = 1000$ Myr is really a lower limit; as the exponential spindown is very slow at these high values for τ , significantly longer timescales are plausible. To improve the estimate on τ and to distinguish between power law and exponential spindown, it is necessary to test the period evolution on longer timescales. This is done by Irwin et al. (2010) using a sample of periods for field stars with $0.1 < M < 0.3 M_{\odot}$ from the MEarth

project¹. Their periods show a wide spread from 0.3 to 150 d, which rules out the power law spindown tested in Fig. 4. In addition, their analysis yields $\tau = 5 - 10$ Gyr for the fastest rotating VLM objects.

6 SUMMARY AND OUTLOOK

The analysis in Sections 4 and 5 can be summarised as follows:

- (i) At ages of 600 Myr, VLM objects with masses below $0.3 M_{\odot}$ are almost exclusively fast rotators with periods of < 2.5 d. This is in stark contrast to higher mass stars ($0.6 - 1.2 M_{\odot}$) which have periods of 7-14 d and results in a sharp break in the period-mass relation at $0.3 - 0.6 M_{\odot}$.
- (ii) In the VLM regime, the periods as well as the scatter in the periods increases with mass. The scatter is significantly larger than for $0.6 - 1.2 M_{\odot}$ stars.
- (iii) Between 100 and 600 Myr VLM objects experience angular momentum losses. However, a single spindown law cannot explain the evolution of upper and lower period limit

¹ A few additional periods for this mass regime are available from Kiraga & Stepien (2007)

simultaneously. Instead, the fast rotators exhibit less rotational braking than the slow rotators. The exponential spindown timescale increases steeply from ~ 500 Myr for $0.3 M_{\odot}$ to several Gyrs at $0.1 M_{\odot}$.

These results are in line with the currently used models for the rotational evolution. As outlined in Sect. 1, most recent papers on this subject use a Skumanich-type $P \propto t^{0.5}$ law for the slow and an exponential law $P \propto \exp(t)$ for the fast rotators. This approach is supported by our new data. In particular, the periods in Praesepe show that VLM objects at 600 Myr rotate much faster than F-K type stars and have not arrived yet to the Skumanich-type spindown tracks.

The physical origin of the empirical findings outlined above is a matter of debate. The breakdown of the Skumanich law around $\sim 0.3 - 0.6 M_{\odot}$ can possibly be understood as a consequence of interior structure. Going from solar-mass stars down to the VLM regime, the convective zone deepens until the objects become fully convective around $0.35 M_{\odot}$ (Chabrier & Baraffe 1997). Assuming that magnetic field generation and properties are a function of interior structure, this could qualitatively explain why VLM objects spend longer on the exponential track than more massive stars.

The mass-dependence of the spindown timescale might actually be a dependence on T_{eff} , as argued in Scholz (2004). With decreasing temperature, the electrical conductivity of the photospheric gas drops as well and the coupling between gas and magnetic field becomes less efficient. This might affect the mass load of the flux tubes and the efficiency of the stellar wind, and explain the strong increase in the spindown timescale at very low masses. It would also provide an explanation for the universally fast rotation of the ultracool L dwarfs (Reiners & Basri 2008).

The positive period-mass trend at very low masses is already seen in very young clusters (e.g. Scholz & Eislöffel 2005), albeit with much more scatter than in Praesepe. Thus, this feature is likely a remnant of the initial conditions. More detailed theoretical work on the magnetic field generation, wind physics, and their connection to angular momentum loss is required to substantiate this interpretation.

Observationally, the current database still has two major flaws that need to be addressed: a) Too few clusters have been monitored with good time sampling and depth. As a result, we are lacking observational constraints in the substellar regime and cannot fully exclude to be affected by bias in the period range and possible environmental effects on rotation, as recently reported by Littlefair et al. (2010). b) Follow-up observations are required for cluster objects with known rotation periods, to exclude contaminating field stars and obtain complementary information about the stellar and magnetic field properties.

ACKNOWLEDGMENTS

We thank the referee, Joel Hartman, for a constructive report that helped to improve the paper. AS would like to thank Philippe Delorme who made his results available prior to publication. BS is supported by RoPACS, a Marie Curie Initial Training Network funded by the European Commission's Seventh Framework Programme. Part of this work was

funded by the Science Foundation Ireland through grant no. 10/RFP/AST2780 to AS.

REFERENCES

- Abazajian K. N., Adelman-McCarthy J. K., Agüeros M. A., Allam S. S., Allende Prieto C., An D., Anderson K. S. J., Anderson S. F., Annis J., Bahcall N. A., et al. 2009, *ApJS*, 182, 543
- Baraffe I., Chabrier G., Allard F., Hauschildt P. H., 1998, *A&A*, 337, 403
- Barnes S. A., 2007, *ApJ*, 669, 1167
- Carpenter J. M., 2001, *AJ*, 121, 2851
- Chaboyer B., Demarque P., Pinsonneault M. H., 1995, *ApJ*, 441, 865
- Chabrier G., Baraffe I., 1997, *A&A*, 327, 1039
- Delfosse X., Forveille T., Perrier C., Mayor M., 1998, *A&A*, 331, 581
- Delorme P., Collier Cameron A., Hebb L., Rostron J., Lister T. A., Norton A. J., Pollacco D., West R. G., 2011, *ArXiv e-prints*
- Dworetzky M. M., 1983, *MNRAS*, 203, 917
- Hambly N. C., Steele I. A., Hawkins M. R. S., Jameson R. F., 1995, *A&AS*, 109, 29
- Hartman J. D., Gaudi B. S., Pinsonneault M. H., Stanek K. Z., Holman M. J., McLeod B. A., Meibom S., Barranco J. A., Kalirai J. S., 2009, *ApJ*, 691, 342
- Hodgkin S. T., Pinfield D. J., Jameson R. F., Steele I. A., Cossburn M. R., Hambly N. C., 1999, *MNRAS*, 310, 87
- Horne J. H., Baliunas S. L., 1986, *ApJ*, 302, 757
- Irwin J., Aigrain S., Bouvier J., Hebb L., Hodgkin S., Irwin M., Moraux E., 2009, *MNRAS*, 392, 1456
- Irwin J., Aigrain S., Hodgkin S., Irwin M., Bouvier J., Clarke C., Hebb L., Moraux E., 2006, *MNRAS*, 370, 954
- Irwin J., Berta Z. K., Burke C. J., Charbonneau D., Nutzman P., West A. A., Falco E. E., 2010, *ArXiv e-prints*
- Irwin J., Bouvier J., 2009, in E. E. Mamajek, D. R. Soderblom, & R. F. G. Wyse ed., *IAU Symposium Vol. 258 of IAU Symposium, The rotational evolution of low-mass stars*. pp 363–374
- Irwin J., Hodgkin S., Aigrain S., Hebb L., Bouvier J., Clarke C., Moraux E., Bramich D. M., 2007, *MNRAS*, 377, 741
- Irwin J., Irwin M., Aigrain S., Hodgkin S., Hebb L., Moraux E., 2007, *MNRAS*, 375, 1449
- Jenkins J. S., Ramsey L. W., Jones H. R. A., Pavlenko Y., Gallardo J., Barnes J. R., Pinfield D. J., 2009, *ApJ*, 704, 975
- Kawaler S. D., 1988, *ApJ*, 333, 236
- Kiraga M., Stepien K., 2007, *AcA*, 57, 149
- Kraus A. L., Hillenbrand L. A., 2007, *AJ*, 134, 2340
- Krishnamurthi A., Pinsonneault M. H., Barnes S., Sofia S., 1997, *ApJ*, 480, 303
- Littlefair S. P., Naylor T., Mayne N. J., Saunders E. S., Jeffries R. D., 2010, *MNRAS*, 403, 545
- Matt S., Pudritz R. E., 2008, *ApJ*, 678, 1109
- Mestel L., 1984, in S. L. Baliunas & L. Hartmann ed., *Cool Stars, Stellar Systems, and the Sun Vol. 193 of Lecture Notes in Physics*, Berlin Springer Verlag, *Angular Momentum Loss During Pre-Main Sequence Contraction*. pp 49–+

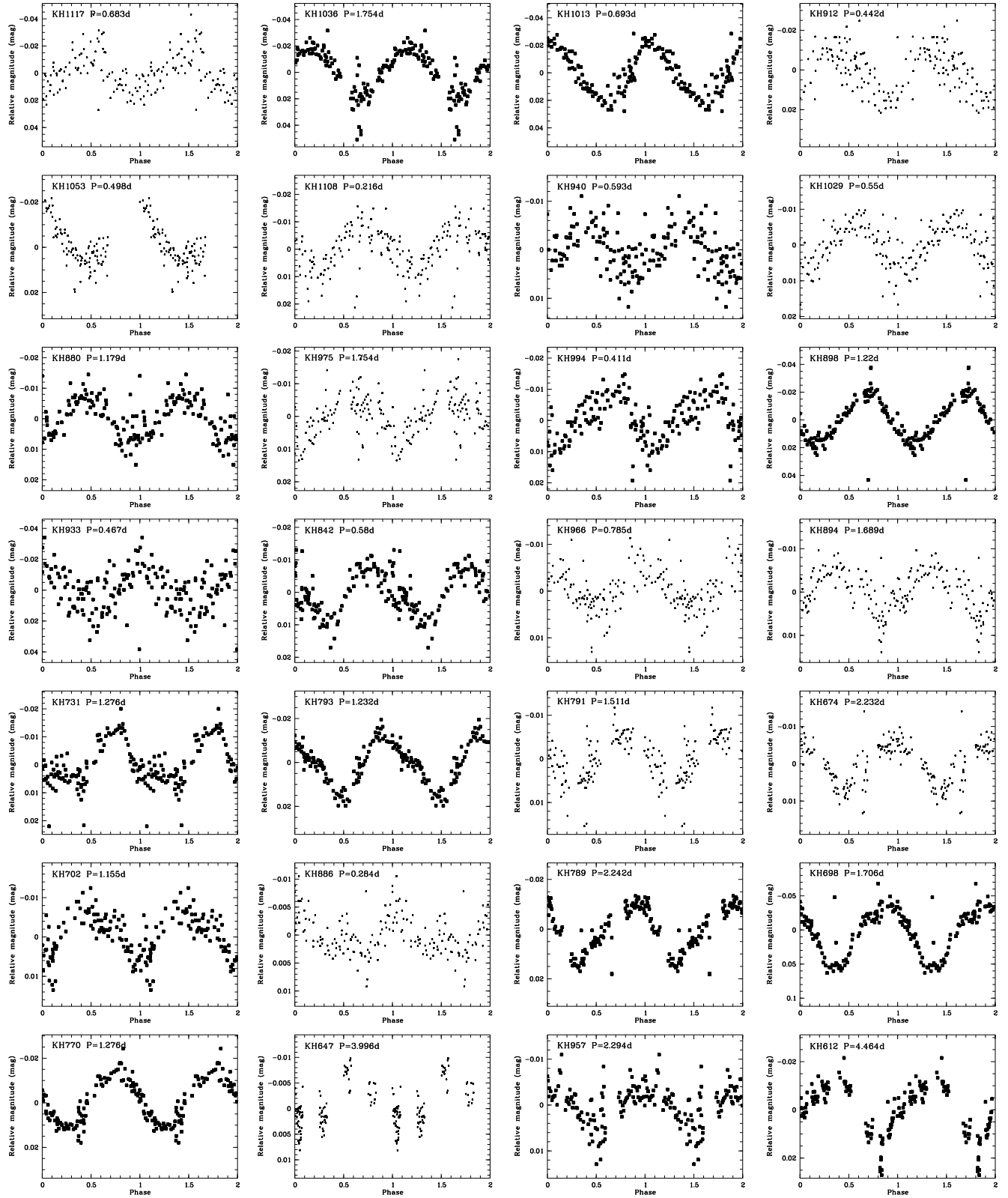


Figure 5. Phased lightcurves for the 49 objects with periods in the order as listed in Table 3, part 1. Ids from Kraus & Hillenbrand (2007) and adopted periods are indicated. The most robust periods ($\text{flag} \geq 4$) are plotted with bold symbols.

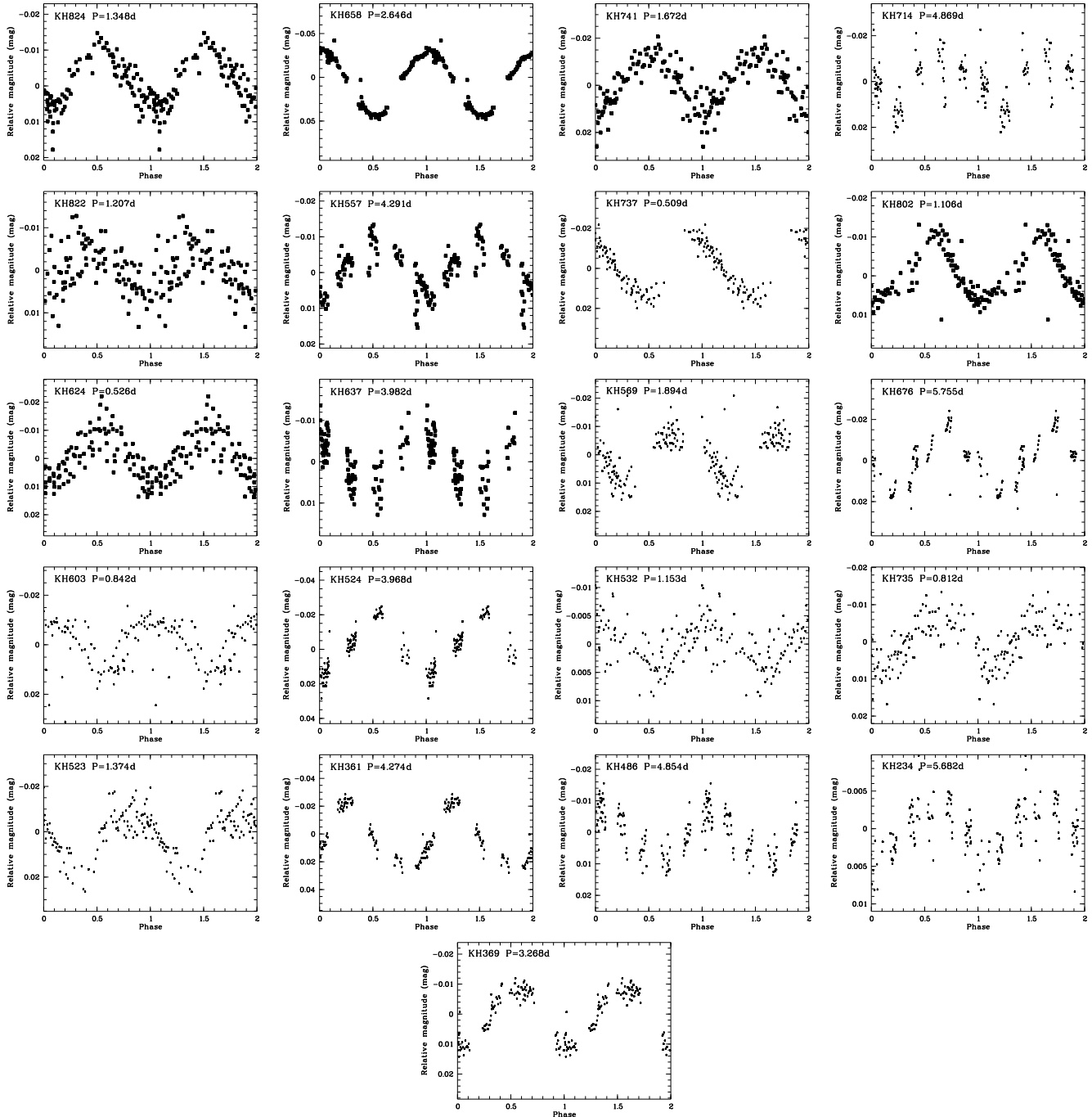


Figure 6. Phased lightcurves for the 49 objects with periods in the order as listed in Table 3, part 2. Ids from Kraus & Hillenbrand (2007) and adopted periods are indicated. The most robust periods ($\text{flag} \geq 4$) are plotted with bold symbols.

Radick R. R., Thompson D. T., Lockwood G. W., Duncan D. K., Baggett W. E., 1987, *ApJ*, 321, 459
 Reiners A., Basri G., 2008, *ApJ*, 684, 1390
 Roberts D. H., Lehar J., Dreher J. W., 1987, *AJ*, 93, 968
 Scargle J. D., 1982, *ApJ*, 263, 835
 Scholz A., 2004, Ph.D. Thesis
 Scholz A., 2009, in E. Stempels ed., *American Institute of Physics Conference Series Vol. 1094 of American Institute of Physics Conference Series, Stellar spindown: From the ONC to the Sun*. pp 61–70
 Scholz A., Eislöffel J., 2004a, *A&A*, 419, 249

Scholz A., Eislöffel J., 2004b, *A&A*, 421, 259
 Scholz A., Eislöffel J., 2005, *A&A*, 429, 1007
 Scholz A., Eislöffel J., 2007, *MNRAS*, 381, 1638
 Skumanich A., 1972, *ApJ*, 171, 565
 Stauffer J. R., Jones B. F., Backman D., Hartmann L. W., Barrado y Navascués D., Pinsonneault M. H., Terndrup D. M., Muench A. A., 2003, *AJ*, 126, 833